

Cold fronts responsible for intense winds in the Santos Basin, Brazilian Southeast Offshore Region

Jamyle MAGALHÃES DA SILVA^{1*}, Fernanda CERQUEIRA VASCONCELLOS¹,
Claudine PEREIRA DEREZYNSKI¹, Amanda REHBEIN² and Michelle SIMÕES REBOITA³

¹ *Universidade Federal do Rio de Janeiro, Instituto de Geociências, Departamento de Meteorologia, Rio de Janeiro, 21941-916, RJ, Brazil.*

² *Universidade de São Paulo, Instituto de Astronomia, Geofísica e Ciências Atmosféricas, Departamento de Ciências Atmosféricas, São Paulo, 05508-090, SP, Brazil.*

³ *Universidade Federal de Itajubá, Instituto de Recursos Naturais, Itajubá, 37500-903, MG, Brazil.*

*Corresponding author; email: jamyle96@gmail.com

Received: April 25, 2022; accepted: November 8, 2022

RESUMEN

Este trabajo tuvo como objetivo identificar las condiciones sinópticas asociadas al paso de frentes fríos que provocan vientos intensos en la cuenca de Santos. Además, se diferenciaron las características atmosféricas de los frentes fríos, los cuales generaron vientos intensos (VINT) y moderados (VMOD) en el área de estudio. Para este propósito, se elaboraron compuestos VINT y VMOD de episodios de frentes fríos. Primero, los casos VINT y VMOD fueron seleccionados a partir de la intensidad de viento a 10 m de altura observada en la boya de Santos, perteneciente al Programa Nacional de Boyas de Brasil. Se analizaron imágenes satelitales y mapas sinópticos de superficie para identificar los sistemas sinópticos responsables de los VINT y VMOD en la boya de Santos, conservando únicamente los casos generados por los frentes fríos. De la comparación entre los compuestos VINT y VMOD, fue posible observar en VINT: (i) un mayor gradiente de presión sobre la cuenca de Santos, lo que provocó intensos vientos registrados en la boya; (ii) una vaguada baroclínica en los niveles medio y alto que llega a la cuenca de Santos y se ubica al oeste del sistema en superficie; (iii) gradientes de 500/1000 hPa de espesor y mayor temperatura de punto de rocío sobre el continente, que llega a la cuenca de Santos e indica la posición del frentes fríos, y (iv) una masa de aire más fría y seca sobre el sur de Brasil. A gran escala, se analizaron los trazados de onda de Rossby, en las cuales se notaron diferentes números de onda para cada compuesto. En VINT el número de onda fue 2, mientras que en VMOD fue 2 y 3. Para los casos de estudio de VINT y VMOD se observaron las principales características encontradas en los respectivos compuestos.

ABSTRACT

This work aimed to identify the synoptic conditions associated with the cold fronts (CFs) passage that causes intense winds in the Santos Basin. Furthermore, the atmospheric characteristics of the CFs, which generated intense (INTW) and moderate (MODW) winds in the studied area, were identified. For this purpose, INTW and MODW composites of CFs episodes were elaborated. First, the INTW and MODW cases were selected from the 10 m wind intensity observed in the Santos buoy, belonging to the Brazilian National Buoys Program. Satellite images and synoptic surface charts were analyzed to identify the synoptic systems responsible for INTW and MODW in the Santos buoy, keeping only the cases generated by CFs. From the comparison between the composites, it was possible to observe in INTW: (i) a stronger pressure gradient over the Santos Basin, with the isobars presenting an almost meridional position near the basin, which caused the intense winds registered in the buoy; (ii) a baroclinic trough at medium and high levels reaching the Santos Basin region, located westward of the surface system; (iii) stronger 1000-500 hPa layer thickness and dew point

temperature gradients over the continent, reaching the Santos Basin region, and (iv) a colder and drier air mass over southern Brazil. On a large scale, the Rossby wave tracings were analyzed, where different wavenumbers were noticed for each composite. In INTW, the wavenumber was 2, while in MODW, it was 2 and 3. Finally, the main characteristics found in the composites were observed in the case studies.

Keywords: cold fronts, strong winds, moderate winds, raytracing.

1. Introduction

Among the meteorological systems that affect the Southeast Region of Brazil and the adjacent ocean, cold fronts are one of the most important because they generally cause significant weather changes and occur more frequently than other transients (Satyamurty et al., 1998; Cavalcanti and Kousky, 2009). During the passage of an intense cold front, it is common to observe an increase in wind speed and change in its direction, an increase in cloudiness, and heavy rains (Cavalcanti and Kousky, 2009; Andrade et al., 2015; Dereczynski and Menezes, 2015; Bonnet et al., 2018; Dereczynski et al., 2019).

The area of interest for this work is the Santos Basin, located over the Atlantic Ocean, for the most part, on the Brazilian southeast coast, extending from Florianópolis (Santa Catarina state) to Cabo Frio (Rio de Janeiro state). The Santos Basin is a vital oil region and the most prominent Brazilian offshore sedimentary basin; it has significant pre-salt exploration fields, whose production began in 2010, and is currently the largest oil and natural gas producer in Brazil (Petrobras, 2022).

Oil and natural gas production has been intensifying in the Santos Basin, and consequently, there is an increase in vessel and helicopter traffic. Thus, it is necessary to understand the behavior of the meteorological systems that affect the region, especially those responsible for generating intense winds. Strong winds can interrupt some operations in the Basin, causing severe delays, for example, the oil transfer from floating production storage and offloading units to tanker vessels or helicopters takeoff and landing.

Most works investigating the passage of cold fronts over the Brazilian continental region focus on precipitation caused during the displacement of these systems (Lima et al., 2010; Reboita et al., 2010; Dolif and Nobre, 2012; Dereczynski et al., 2017; Bonnet et al., 2018; Escobar et al., 2019). This is justifiable because heavy rainfall events are responsible for landslides, floods, river overflows, and other

problems that pose a high risk to the population, which may cause loss of life and material goods.

The main characteristics identified in the cold fronts associated with heavy rainfall events are: (i) behind the cold front, intense migratory flows high on the surface; (ii) strong moisture convergence associated with the cold front, and (iii) great baroclinic troughs at 500 and 250 hPa (Moura et al., 2013; Andrade and Cavalcanti, 2018; Bonnet et al., 2018). Franco et al. (2020) analyzed 23 intense wind events that caused electrical power transmission towers to fall in Paraná state between 1980 and 2017. Three of the four synoptic patterns identified were associated with a strong pressure gradient over the region and two were related to a cold front south of the study region.

Some cold front events associated with heavy rainfall may be connected to wave trains coming from the Pacific Ocean (Andrade and Cavalcanti, 2018), related to different phases of teleconnection patterns. Andrade and Cavalcanti (2018) confirmed the influence of the Southern Annular Mode (SAM) and the Madden-Julian Oscillation (MJO) in the passage of cold fronts with light and heavy precipitation. The cold fronts were classified based on the precipitation amount of three days. By ranking the total precipitation in this period, cases with a percentile below 5% were called dry extremes, and those with a percentile above 95% were wet extremes. The three-day period includes pre- and post-frontal precipitation occurrence. The authors related the positive (negative) SAM phase to wet (dry) cases.

Regarding the MJO, they showed that convection in Indonesia and eastern Brazil have opposite relationships. When convection is strong in Indonesia, it reduces in the east of Brazil and vice versa. Caldas et al. (2020) also verified that a combination of different SAM, El Niño Southern Oscillation (ENSO) phases, and Antarctic Ocean ice anomalies in Bellinghshausen-Amundsen (BAS) and Weddel (WDS) seas influence the cold fronts tracks over South America.

In the Santos Basin region, the maximum frequencies occurred for negative SAM, El Niño, and minimum sea ice extension in the BAS combination and positive SAM, La Niña, and maximum sea ice extension in the WDS combination (Caldas et al., 2020).

This work aims to identify the characteristics of the cold fronts responsible for generating intense winds (INTW) cases in the Santos Basin by comparing them with moderate winds (MODW) cases. Furthermore, another objective is to identify large-scale patterns contributing to the occurrence of INTW cases. Section 2 describes the data and methodology used. The results are in section 3 and the conclusions are in section 4.

2. Data and methodology

2.1 Case selection and composite preparation

The 10-m wind intensity and direction (W10M) in the Santos buoy, belonging to the Brazilian National Buoys Program (PNBOIA), were analyzed to select the cases of cold fronts that caused intense winds in the Santos Basin. The W10M data periods available extend from 04/12/2011 to 12/31/2011 and 01/01/2014 to 07/15/2017, totaling 1555 days. First, the cold fronts that caused winds higher than 10 m s^{-1} in the Santos buoy were identified. Infrared images from the Geostationary Operational Environmental Satellite (GOES-12 and GOES-13), obtained by the Division of Satellites and Environmental Systems of the National Institute for Space Research, were analyzed to identify cold fronts associated with days where $W10M > 10 \text{ m s}^{-1}$ based on their cloudiness aspect. Besides, synoptic surface charts, prepared every 6 h by the Weather Forecasting Group of the National Institute for Space Research, were used to ensure the presence of the cold fronts. In this way, all cases of $W10M > 10 \text{ m s}^{-1}$ that occurred during the passage of cold fronts were selected and organized in W10M descending order. Thus, the ones above the 99th percentile ($\geq 13.7 \text{ m s}^{-1}$) are named intense wind (INTW) cases. It is noteworthy that the Beaufort wind scale classifies winds above 14.4 m s^{-1} as near gale (Brasil, 2021). Cases in which W10M is higher than or equal to the 70th percentile and less than the 90th percentile ($8.6 \leq W10M < 10.8 \text{ m s}^{-1}$) are considered moderate wind (MODW) cases. Thus, 16 INTW cases and 10 MODW cases were identified.

In order to standardize the number of cases in both categories, just the 10 most intense cases above the 99th percentile for the INTW classification were used.

To identify the main characteristics of cold fronts that cause intense winds in the Santos Basin, composites were elaborated at the synoptic time closest to the occurrence of the most intense winds ($t = 0$) in each event for the categories described above. Also, the same composites were elaborated 24 h before the occurrence of the most intense winds ($t = -24$) in each event (see these results in Figs. S1 and S2 in the supplementary material). CFSR outputs from the National Centers for Environmental Prediction Reanalysis, v. 2 (Saha et al., 2014), were used for each case. The spatial resolution of this reanalysis data is 0.5° latitude by 0.5° longitude, and the temporal resolution is 6 h. The meteorological variables used were: (i) mean sea level pressure (MSLP, in hPa); (ii) 500 and 1000 hPa geopotential height to build the thickness field between 500 and 1000 hPa (THC500_1000, in gpm); (iii) 2-m dewpoint temperature (DT2M, in $^\circ\text{C}$); (iv) 10-m zonal and meridional wind components, and (v) 500 and 200 hPa zonal and meridional wind components (in m s^{-1}). The t-Student test was applied with 95% statistical confidence to the composites (Wilks, 2006).

2.2 Cyclone trajectory

A script identified the cyclones' trajectory associated with each cold front searching the minimum MSLP value over the South Atlantic region to locate the low-pressure centers. This analysis considered the day of the most intense wind occurrence and the day before and after. After this step, the position of the low-pressure centers was identified every 6 h, following the reanalysis temporal resolution. Thus, the cyclones' tracks were elaborated for each case.

2.3 Raytracing

Raytracing v. 0.1.0 (Rehbein et al., 2020) was used to obtain the Rossby wave trajectories for the INTW and MODW composites. It consists of a tool developed in the R language (R Core Team, 2021) available in its official repository and GitHub. This methodology is based on the theoretical development of Hoskins and Ambrizzi (1993), and it is similar to Yang and Hoskins (1996) for using the second-order Runge-Kutta method to get group velocities over

the integration period. The raytracing obtains the absolute vorticity (β) meridional gradient values, the stationary waves' total number (Ks), and the Rossby wave traces for different initial conditions.

The data used is the 200 hPa zonal wind average (u_{200}) from the CFSR v. 2 reanalysis (Saha et al., 2014), calculated in the same way as the composites for INTW and MODW. However, the data were interpolated using the conservative method (Jones, 1999) for a resolution of 2.5° to avoid signal noise from smaller-scale systems during tracking.

Raytracing makes it possible to look for the trajectory followed by the Rossby wave through different initial conditions and varied sources. In this study, waves generated between 175° - 110° W and 25° - 50° S were tracked, with a distance of 5° between the points, the total integration time of 10 days (program default), and total wave numbers (K) 2, 3, and 4.

After this, wave traces that crossed the Santos Basin at any point were selected. In INTW, the trajectories that passed through the Santos Basin had $K = 2$. In MODW, they had $K = 2, 3$.

3. Results

3.1 Composite analysis

Information on the INTW and MODW cases registered in the Santos buoy from 04/12/11 to 12/31/2011 and 01/01/2014 to 07/15/2017 are listed in Table I. Note that most INTW cases occurred in 2016 (five cases), followed by 2011 (four cases) and 2015 (one occurrence). Regarding seasonality, seven of the 10 INTW cases occurred in winter (JJA), followed by fall (MAM, 2 cases) and spring (SON, 1 case). There were no INTW cases in the summer (DJF) since the penetration of strong cold air masses, which could

Table I. INTW and MODW selected cases caused by cold fronts in the Santos buoy, in speed-decreasing order.

Intense wind cases (INTW)			Moderate wind cases (MODW)		
Event time and day ($t = 0$; $t = -24$)	The most intense wind recorded		Event time and day ($t = 0$; $t = -24$)	The most intense wind recorded	
	Speed (m s^{-1})	Direction ($^\circ$)		Speed (m s^{-1})	Direction ($^\circ$)
21 UTC 08/21/2016 ($t = 0$: 18:00 UTC 08/21/2016; $t = -24$: 18:00 UTC 08/20/2016)	17.3	222	10:00 UTC 08/24/2015 ($t = 0$: 12:00 UTC 08/24/2015; $t = -24$: 12:00 UTC 08/23/2015)	10.7	235
20:00 UTC 11/18/2016 ($t = 0$: 18:00 UTC 11/18/2016; $t = -24$: 18:00 UTC 11/17/2016)	16.6	204	7:00 UTC 05/09/2014 ($t = 0$: 06:00 UTC 05/09/2014; $t = -24$: 06:00 UTC 05/08/2014)	10.6	164
16 UTC 06/04/2011 ($t = 0$: 18:00 UTC 06/04/2011; $T = -24$: 18:00 UTC 06/03/2011)	16.5	209	22 UTC 05/26/2011 ($t = 0$: 00:00 UTC 05/27/2011; $t = -24$: 00:00 UTC 05/26/2011)	10.4	185
11 UTC 04/27/2016 ($t = 0$: 12 UTC 04/27/2016; $t = -24$: 12:00 UTC 04/26/2016)	16.5	252	15 UTC 07/22/2011 ($t = 0$: 12:00 UTC 07/22/2011; $t = -24$: 12:00 UTC 07/21/2011)	10.1	182

Table I. INTW and MODW selected cases caused by cold fronts in the Santos buoy, in speed-decreasing order.

Intense wind cases (INTW)			Moderate wind cases (MODW)		
Event time and day (t = 0; t = -24)	The most intense wind recorded		Event time and day (t = 0; t = -24)	The most intense wind recorded	
	Speed (m s ⁻¹)	Direction (°)		Speed (m s ⁻¹)	Direction (°)
22 UTC 06/07/2011 (t = 0: 00:00 UTC 06/08/2011; t = -24: 00:00 UTC 06/07/2011)	16.4	306	01 UTC 09/12/2011 (t = 0: 00:00 UTC 09/12/2011; t = -24: 00:00 UTC 09/11/2011)	10.0	157
06 UTC 08/10/2011 (t = 0: 06:00 UTC 08/10/2011; t = -24: 06:00 UTC 08/09/2011)	16.0	107	19 UTC 12/01/2011 (t = 0: 18:00 UTC 12/01/2011; t = -24: 18:00 UTC 11/30/2011)	9.9	150
10 UTC 08/27/2015 (t = 0: 12:00 UTC 08/27/2015; t = -24: 12:00 UTC 08/26/2015)	16.0	112	09 UTC 05/02/2011 (t = 0: 06:00 UTC 05/02/2011; t = -24: 06:00 UTC 05/01/2011)	9.9	143
02 UTC 07/04/2011 (t = 0: 00:00 UTC 07/04/2011; t = -24: 00:00 UTC 07/03/2011)	14.9	199	19 UTC 11/23/2014 (t = 0: 18:00 UTC 11/23/2014; t = -24 18:00 UTC 11/22/2014)	9.9	211
14 UTC 05/23/2016 (t = 0: 12:00 UTC 05/23/2016; t = -24: 12:00 UTC 05/22/2016)	14.7	302	22 UTC 05/12/2011 (t = 0: 00:00 UTC 05/13/2011; t = -24: 00:00 UTC 05/12/2011)	9.0	203
19 UTC 07/16/2016 (t = 0: 18:00 UTC 07/16/2016; t = -24 18:00 UTC 07/15/2016)	14.7	299	00 UTC 04/21/2014 (t = 0: 00:00 UTC 04/21/2014; t = -24: 00:00 UTC 04/20/2014)	8.8	59

generate strong pressure gradients, are unusual at this time of year. Most MODW cases occurred in 2011 (six cases), followed by 2014 (three cases) and 2015 (one event). Five of the 10 cases occurred in fall, followed by winter and spring (two cases in each season) and summer (one occurrence). The W10M oscillated between 14.7 and 17.3 m s⁻¹ during INTW

and between 8.8 and 10.8 m s⁻¹ during MODW, with the maximum intensity recorded after the cold front passage in most cases since the wind direction is from the south quadrant (Table I).

Figure 1 shows the MSLP and W10M fields, the THC500_1000 and DT2M fields for INTW and MODW composites, and also the difference between

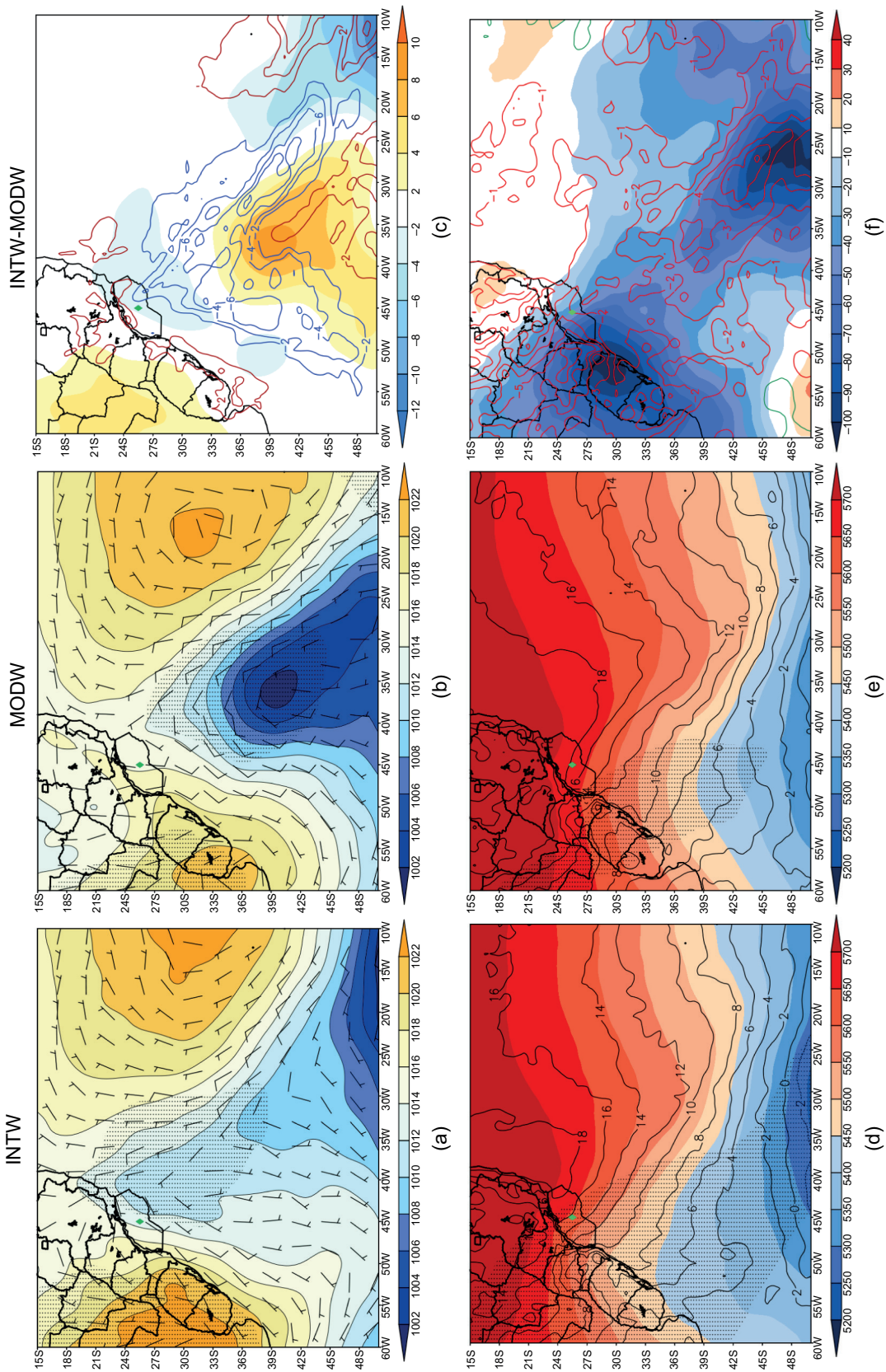


Fig. 1. MSLP (hPa, shaded) and W10M (m s^{-1} , barb) composites (top row), and THC500_1000 (gpm, shaded) and DT2M ($^{\circ}\text{C}$, contour) composites (bottom row) at the synoptic time closest to the occurrence of the most intense winds in each event ($t = 0$). (a) and (d) INTW, (b) and (e) MODW, (c) and (f) INTW-MODW. (c) W10M (m s^{-1} , contour) difference between INTW-MODW. Areas with a confidence level of 95% in dots (t-Student test) for MSLP (top row) and layer thickness (bottom row). The Santos buoy location is indicated in the green diamond.

INTW-MODW at the synoptic time closest to the occurrence of the most intense winds in each event ($t = 0$). In Figure 1, INTW cases are in the left column, MODW cases are in the middle column, and the difference between them (INTW-MODW) is in the right column. Figure 2 shows the MSLP gradient and 500 and 200 hPa streamline field composites. The INTW (MODW) composite is in the left (right) column. In Figures 1 and 2, dotted areas show where there is statistical significance at the 95% level. In other words, the composite is representative of each case in areas with a confidence range of at least 95%.

In the INTW composite (Fig. 1a), it is possible to observe the frontal trough extending meridionally over the Atlantic Ocean, reaching the north of the Santos Basin, with 1010 hPa. In addition, a post-frontal anticyclone acts over the continent, with pressure values above 1022 hPa. There is statistical significance in both systems. Under these conditions, a strong pressure gradient (Fig. 2a) over Santos Basin can be observed, with values up to $1.6 \times 10^{-3} \text{ Pa m}^{-1}$ in the south of Santos Basin and the isobars presenting an almost meridional position near the basin. As a result, winds parallel

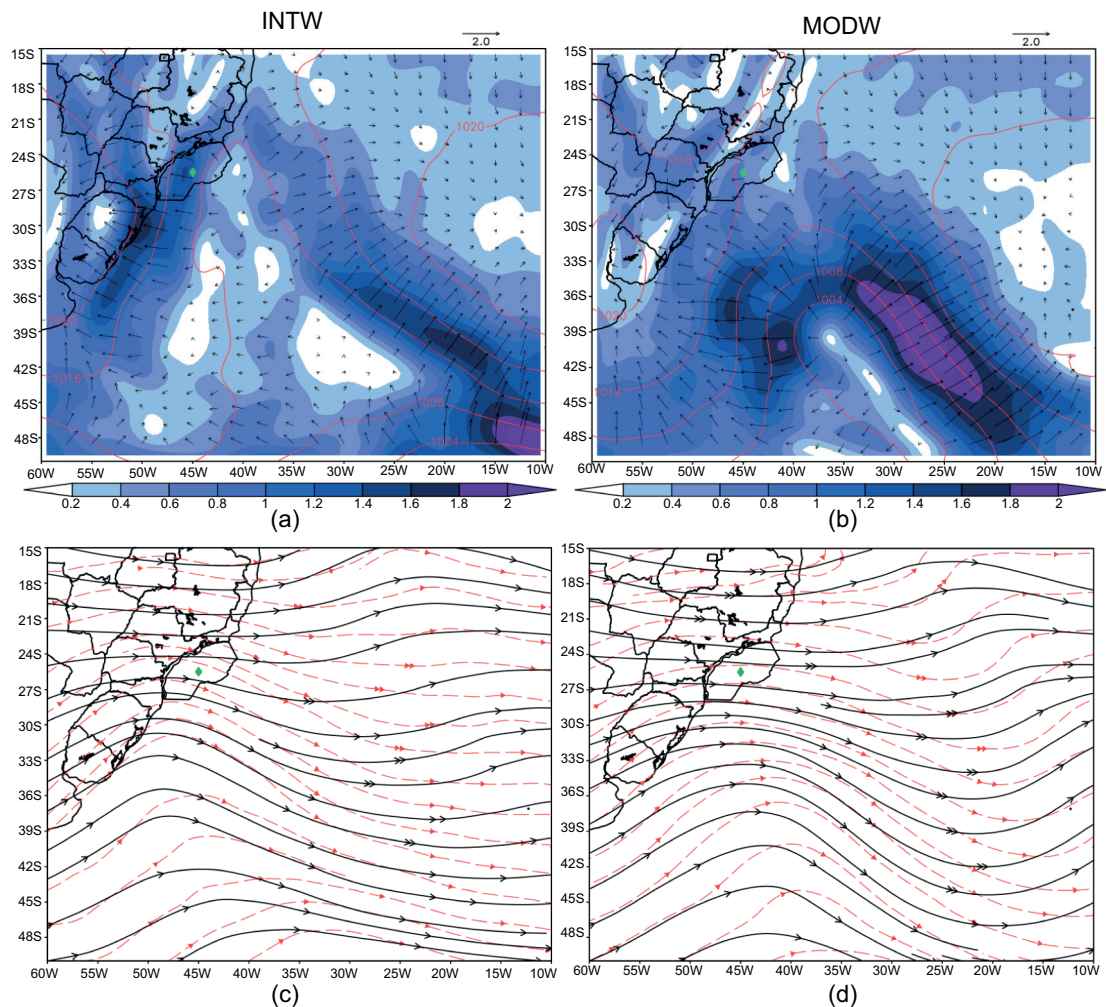


Fig. 2. Pressure gradient ($10^{-3} \text{ Pa m}^{-1}$, vector and shading) with MSLP (red line in hPa) composites (top row) and streamline at 500 hPa (dashed red) and 200 hPa (solid black) composites (bottom row) at the synoptic time closest to the occurrence of the most intense winds in each event ($t = 0$). (a) and (c) INTW, (b) and (d) MODW. Santos buoy location is indicated in the green diamond.

to the coast and over the Santos Basin are recorded in the Santos buoy. The almost meridional isobars over the region are noteworthy, generating intense southerly winds in the study area.

The MODW composite (Fig. 1b) has a low-pressure center with 1002 hPa over the Atlantic Ocean (around 40° S/35° W), making the MSLP lower in this region than in the INTW composite and with statistical significance, showing that this pattern is similar in most cases. However, the frontal trough that reaches the Santos Basin and the post-frontal anticyclone over the continent is not as intense as in the INTW composite, generating a weaker pressure gradient over the Santos Basin (Fig. 2b) of 0.8×10^{-3} Pa/m. The isobars are also not as meridional over the Santos Basin. So, winds recorded in the Santos buoy were not as intense in the MODW composite. Figure 1c shows that over the Santos Basin, the pressure in INTW is lower than in MODW (between 2 and 4 hPa), and it is higher than MODW over the continent (up to 6 hPa) and the ocean around 40° S/35° W (up to 9 hPa).

The strong THC500_1000 and DT2M gradients show the cold front position over the Santos Basin region, getting into the continent in INTW (Fig. 1d). Meanwhile, in MODW the cold front is more oceanic, located over the southern Santos Basin (Fig. 1e). Besides, the air mass advancing over southern Brazil in INTW is colder and drier. It penetrates further into the continent (Fig. 1f), generating THC500_1000 values around 100 gpm (lower in INTW than in MODW) over the Rio Grande do Sul State, and DT2M values 4 °C lower in INTW than in MODW.

In Figure 2c, at 500 (dashed red) and 200 hPa (solid black), the baroclinic structure of the INTW systems in the Santos Basin can be seen. At both levels, the trough has greater amplitude, reaches the Santos Basin region, and is located west of the surface cold front, providing dynamic support for the intensification of cold fronts. In MODW (Fig. 2d), the trough reaches only the southern Santos Basin with a smaller amplitude than INTW, indicating that the frontal waves were more restricted to this region, collaborating with the surface systems' displacement over the ocean.

The same fields shown in Figures 1 and 2 for $t = 0$ are shown in Figures S1 and S2 in the supplementary material for $t = -24$. In the INTW composite (Fig. S1a), a relatively low-pressure area (1012-

1014 hPa) extends over the Atlantic Ocean, associated with a low-pressure area of 1004 hPa in 49° S/30° W. The post-frontal anticyclone is located south of Uruguay, with MSLP above 1020 hPa, with statistical significance. The pressure gradient (Fig. S2a) over the Santos Basin is weak, around 0.6×10^{-3} Pa m⁻¹. In the MODW composite (Fig. S1b), the low-pressure center over the Atlantic Ocean is 1004 hPa (around 39° S/49° W), producing a stronger pressure gradient when compared to INTW over the Atlantic Ocean near this center and also over the Santos Basin (around 0.8×10^{-3} Pa m⁻¹). Also, the South Atlantic Subtropical High is displaced to the southwest, producing stronger northerly winds than INTW cases. Figure S1c is similar to Figure 1c, except that systems are displaced to the south in $t = -24$.

In Figures S1d and S1e, it is possible to observe THC500_1000 and DT2M stronger gradients over South Brazil, with a deeper thickness (THC500_1000), and colder and drier air (DT2M) in INTW cases compared to MODW cases (Fig. S1f).

In Figure S2c, both troughs (500 and 200 hPa) are tilted to the left and almost in phase in INTW cases. The troughs in MODW show a baroclinic structure, and they are more meridional than in INTW.

Comparing the meteorological fields in Figure S1 to Figure 1 and in Figure S2 to Figure 2, a southern position of the system in $t = -24$ compared to $t = 0$ is evident. However, the differences between INTW and MODW composites are not as expressive in $t = -24$ as in $t = 0$. This result shows the difficulty in forecasting intense winds at the Santos Basin when the cold front is still located south of the basin, 24 h before its penetration in the studied region.

Figure 3 shows the cyclone centers' trajectory associated with the cold fronts analyzed in both composites (INTW and MODW). Each color represents one of the selected cases. The starting point is close to the continent, and the ending over the ocean. In INTW (Fig. 3a), the cyclones are farther apart. It justifies that the MSLP composite does not have a well-marked center with low mean pressure but rather a trough (INTW composite, Fig. 1a). In MODW (Fig. 3b), the cyclones are concentrated southward of 30° S with similar trajectories. It makes the MSLP composite more defined, thus enabling the identification of a center of low pressure in the average of all the cases (MODW composite, Fig. 1b).

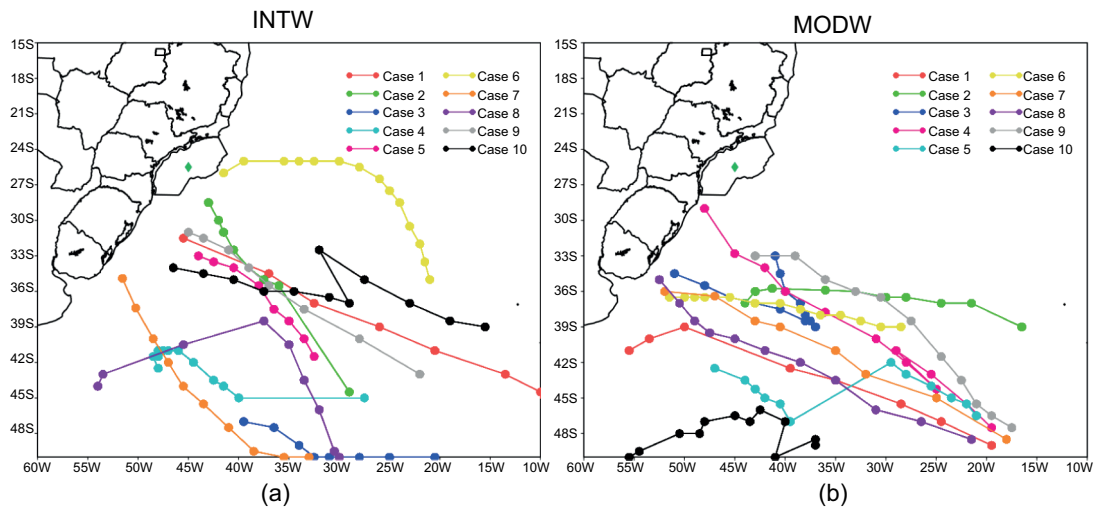


Fig. 3. Cyclones' trajectories detected from the CFSR reanalysis: (a) INTW cases and (b) MODW cases. Santos buoy location is indicated in the green diamond.

3.2 Large scale analysis

To identify INTW and MODW patterns on a large scale, geopotential height at 500 hPa, its anomaly (Fig. 4), and 200 hPa meridional winds (v_{200} , Fig. 5) fields were elaborated. Figure 4a shows significant negative anomalies in almost the whole middle latitude circle, which indicates a negative SAM phase.

Besides that, Figure 3a shows the cyclones' trajectories further north over the ocean, characteristic of the negative SAM (Reboita et al., 2009). In MODW, there is no clear sign of the SAM performance (Fig. 4b). Instead, the middle latitudes present an alternation between positive and negative anomalies on these latitudes. In the INTW, it is possible to observe a

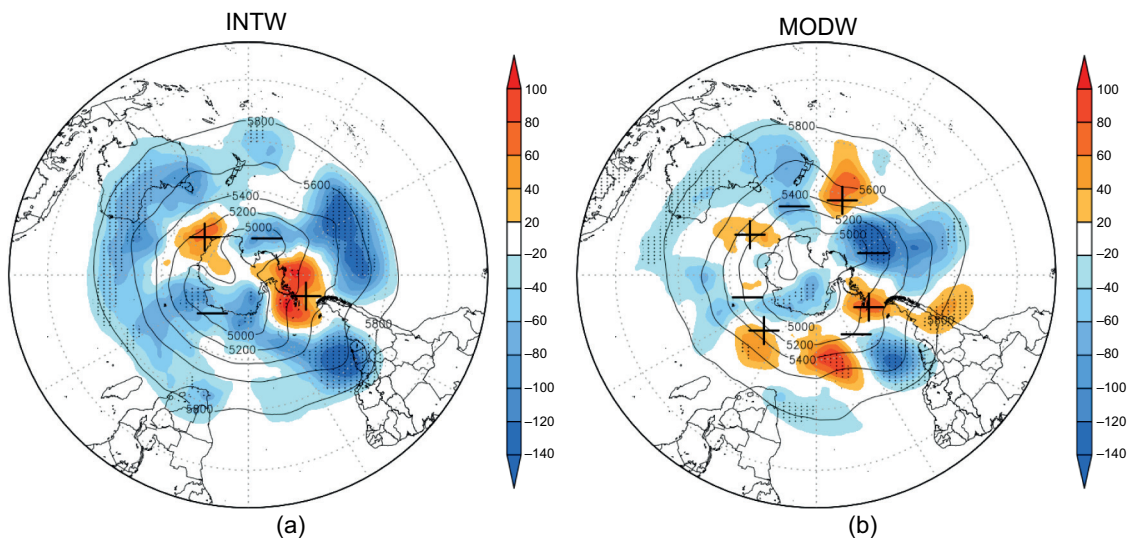


Fig. 4. Geopotential height (gpm, solid lines) and geopotential anomaly (gpm, shaded) composite at 500 hPa for: (a) INTW, (b) MODW. Areas with a confidence level of 95% in dots (t-Student test) for geopotential anomaly. Positive (+) and negative (-) signs symbolize positive (ridges) and negative (troughs) geopotential anomalies, indicating the number of waves.

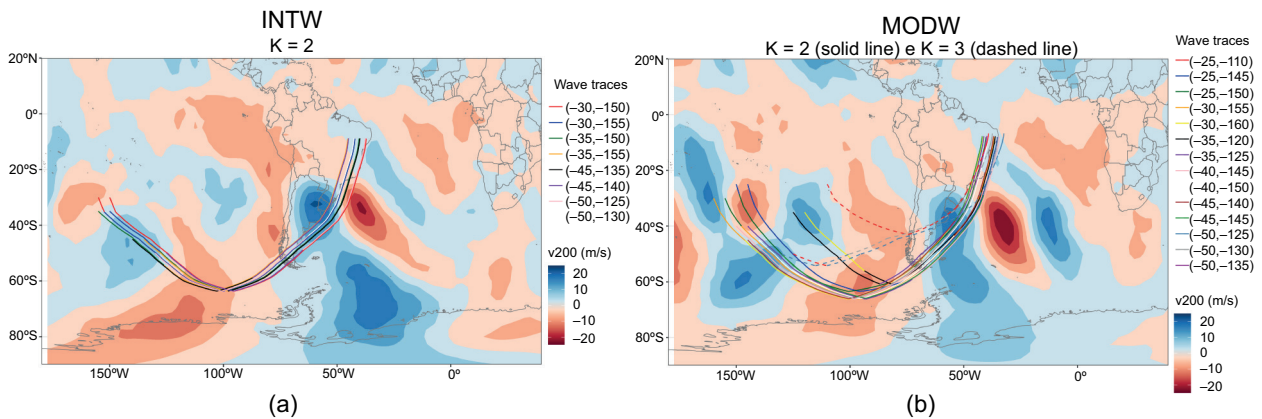


Fig. 5. v_{200} (m s^{-1}) composite and paths followed by Rossby waves with $K = 2$ (solid line) and $K = 3$ (dashed line) for: (a) INTW, (b) MODW.

significant negative anomaly over the east coast of South America, reaching the Santos Basin. Also, there is a large trough from the south of South America to southeast Brazil (Fig. 4a). In MODW (Fig. 4b) there is also a significant negative anomaly near South America. However, it is a bit further away from the continent. In addition, the trough is over the ocean and has less amplitude than in INTW.

Both composites registered a wave train from the Pacific to the Atlantic. Nevertheless, the anomalous centers in MODW seem to be shifted eastward concerning INTW, which can be explained by the wavenumber difference at higher latitudes (Fig. 4). While in INTW (Fig. 4a) the composite shows a low wavenumber pattern (wave 2), in MODW (Fig. 4b) there is higher wavenumber pattern (wave 4).

Figure 5 shows the paths followed by Rossby waves in INTW (Fig. 5a) and MODW (Fig. 5b), from a region at around $40^{\circ}\text{S}/145^{\circ}\text{W}$. In this region south quadrant winds are observed at 200hPa in INTW (Fig. 5a). In MODW (Fig. 5b) there are northerly winds. The v_{200} composite also shows that the wavenumber is higher in MODW (Fig. 5). In INTW there are only paths with $K = 2$ (Fig. 5a). In MODW, there are trajectories with $K = 2, 3$, where the curvature is wider than $K = 2$. The $K = 3$ and some of the $K = 2$ trajectories starting near the continent may have favored the cold fronts in MODW to be more oceanic (Fig. 5b). Thus, there is a relationship between the Rossby wave formation region over the South Pacific and the

cold fronts that moved over the Santos Basin. This suggests that remote characteristics can influence the circulation pattern, displacing the cold front passages over South America and the adjacent Atlantic, thereby affecting the Santos Basin. Several authors have already discussed this remote influence on South America through wave trains (e.g., Vasconcellos and Cavalcanti, 2010; Coelho et al., 2016; Vasconcellos and Souza, 2022).

3.3 Case studies

The case studies were selected based on data from the Santos buoy from 05/03/2018 to 07/12/2018. The selection criteria for the fronts and the INTW and MODW thresholds were the same in the composites. The first case was a cold front that passed through the Santos Basin on 07/03/2018. The 18:00 UTC satellite image (Fig. 6a) shows low cloudiness over the Santos Basin associated with the cold front, which moves over the ocean. It caused winds of up to 19.8 m s^{-1} recorded in the Santos buoy at 16:00 UTC. In the second case, the cold front passed through the Santos Basin on 05/12/2018, causing winds of 9.5 m s^{-1} recorded in the Santos buoy at 15:00 UTC. Its associated cloudiness can be seen in Figure 6b. Therefore, the first case is an INTW (above the 99th percentile threshold) and it will be called INTW Case. The second one is a MODW case (between the 90th and 70th percentiles thresholds) and it will be called MODW Case. The fields are for the closest time to the occurrence of the strongest wind.

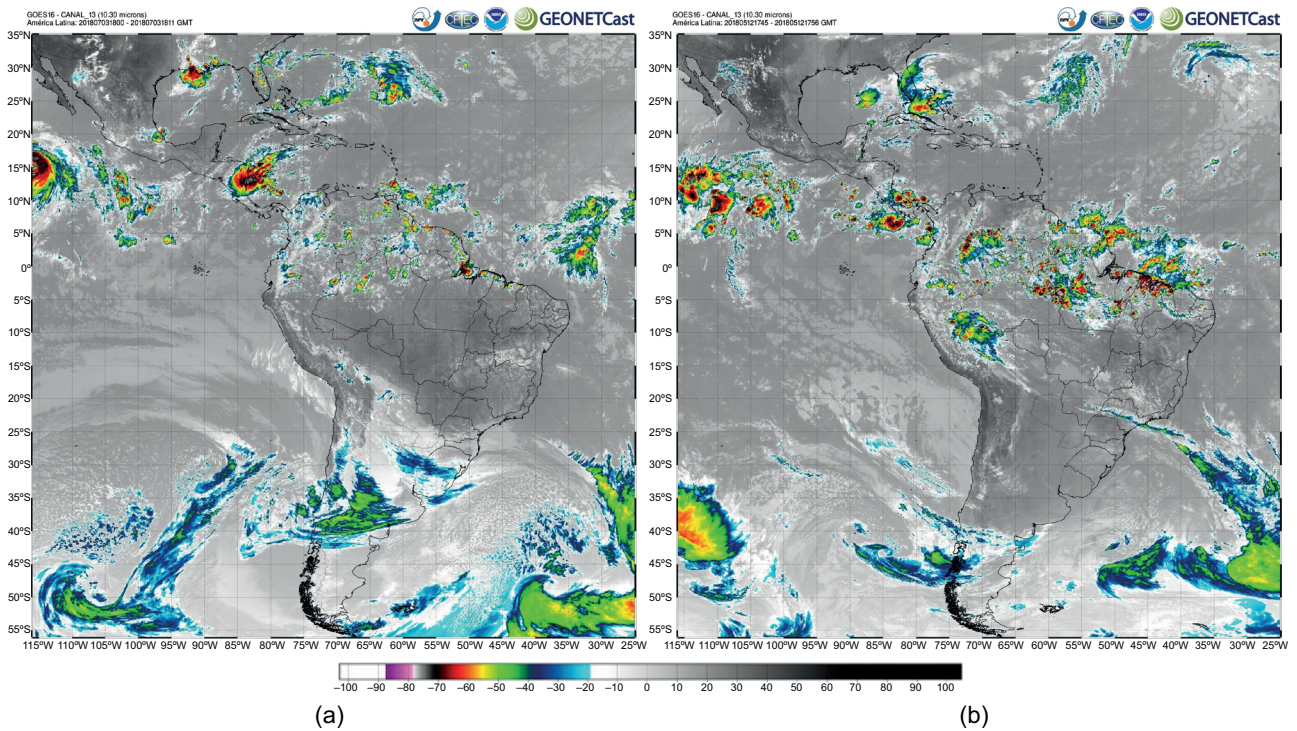


Fig. 6. GOES-16 satellite images on channel 13 (infrared) for: (a) 07/03/2018 at 18:00 UTC (INTW Case); (b) 05/12/2018 at 18:00 UTC (MODW Case).

On the MSLP field, the INTW Case (Fig. 7a) shows the cold front with the pressure trough close to the north of the Santos Basin, similar to that seen in the INTW composite (Fig. 1a), with 1012 hPa, indicating the cold front position. The low-pressure center with less than 964 hPa is over the ocean at around 48° S/ 37° W. The post-frontal anticyclone is over the continent, around 60° W, with a value of up to 1028 hPa (Fig. 7a). As seen in Figure 1a, there is also a post-frontal anticyclone and intense frontal trough, with meridional isobars in the INTW case. Under these conditions, a strong pressure gradient with a module up to 2×10^{-3} Pa m^{-1} and east-west orientation is observed over the Santos Basin (Fig. 7c), causing the intense winds recorded in the Santos buoy. In the MODW Case (Fig. 7b), the 980 hPa low-pressure center over the ocean, close to 42° S/ 35° W, is weaker than in the INTW Case. The frontal trough also reaches the north of the Santos Basin; nonetheless, it is more intense than in the INTW case. It opposes what was observed in the MODW composite (Fig. 1b), with a value between 1008 and 1012 hPa. The post-frontal anticyclone over

the continent (at 30° S/ 58° W) is weaker than in the INTW Case, with 1020 hPa at its center. It causes a weaker pressure gradient over the Santos Basin, with a module lower than 1×10^{-3} Pa m^{-1} and less zonal orientation than in the INTW case (Fig. 7d), responsible for the moderate winds recorded in the buoy. It should be reiterated that the field's time is after the event occurs in both cases.

At medium (dashed red) and high (solid black) levels, the baroclinic trough of the INTW Case is lower and is located east of the Santos Basin, over the ocean. At this time, the system was in occlusion (Fig. 7e). This large and deep meridional trough is one of the main features observed in the INTW composite (Fig. 2a). In the MODW Case (Fig. 7f), the baroclinic trough is also over the ocean, east of the BS. However, it has a lower amplitude and intensity than in the INTW Case (Fig. 7e). These trough characteristics with lower amplitude and weaker intensity at high levels are similar to those observed in MODW (Fig. 2b).

The strong THC500_1000 and DT2M gradients (Fig. 7g, h) indicate that the cold front is over the

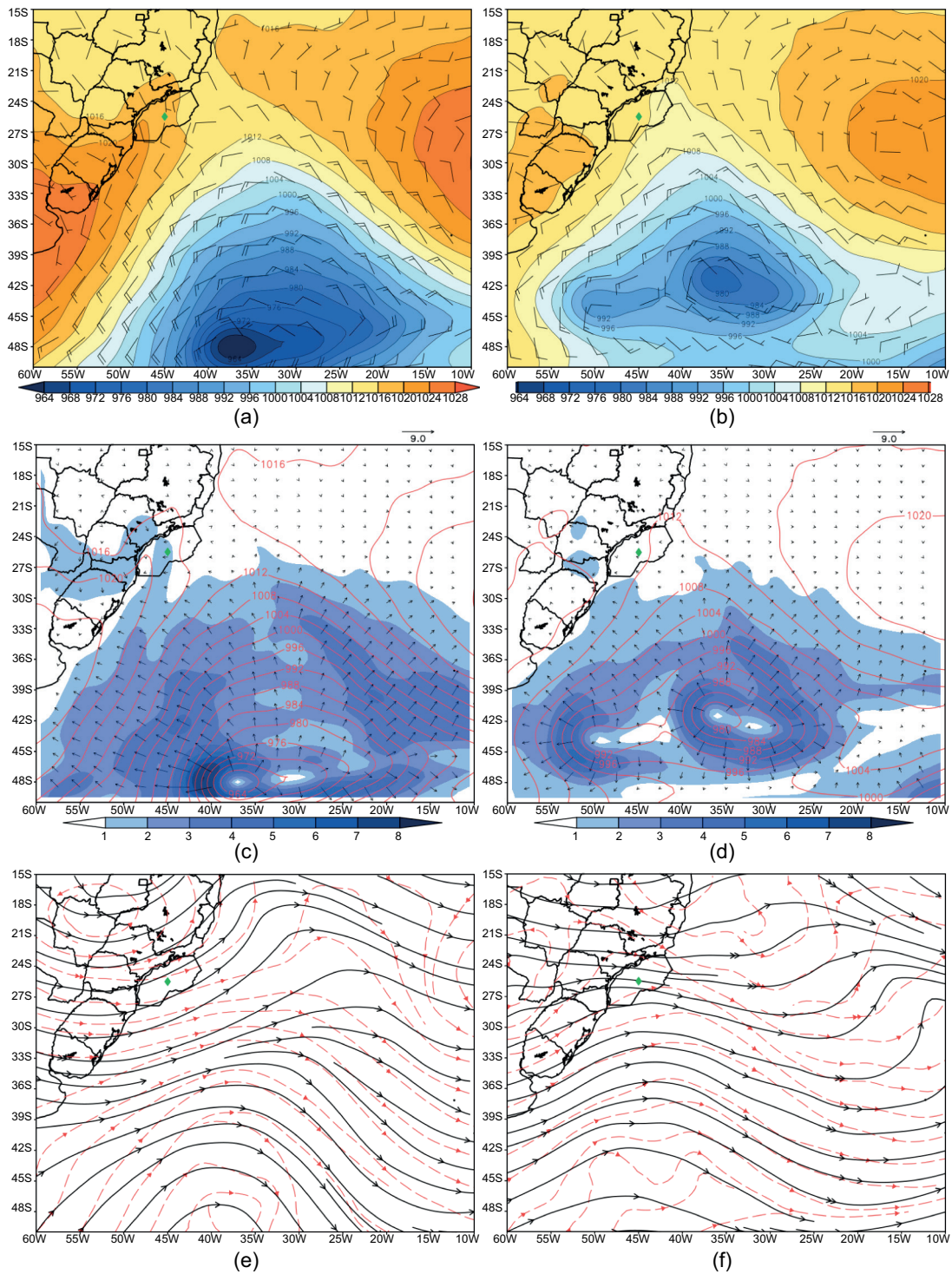


Fig. 7. (a) and (b) MSLP (hPa, shaded) and W10M (m s⁻¹, barbs); (c) and (d) pressure gradient (10⁻³ Pa m⁻¹, vectors and shading) and MSLP (hPa, red outline); (e) and (f) streamline at 500 hPa (dashed red) and 200 hPa (solid black). Fields are for INTW Case (07/03/2018 at 18:00 UTC (left column) and MODW Case (05/12/2018 at 18:00 UTC (right column). Santos buoy location is indicated in the green diamond.

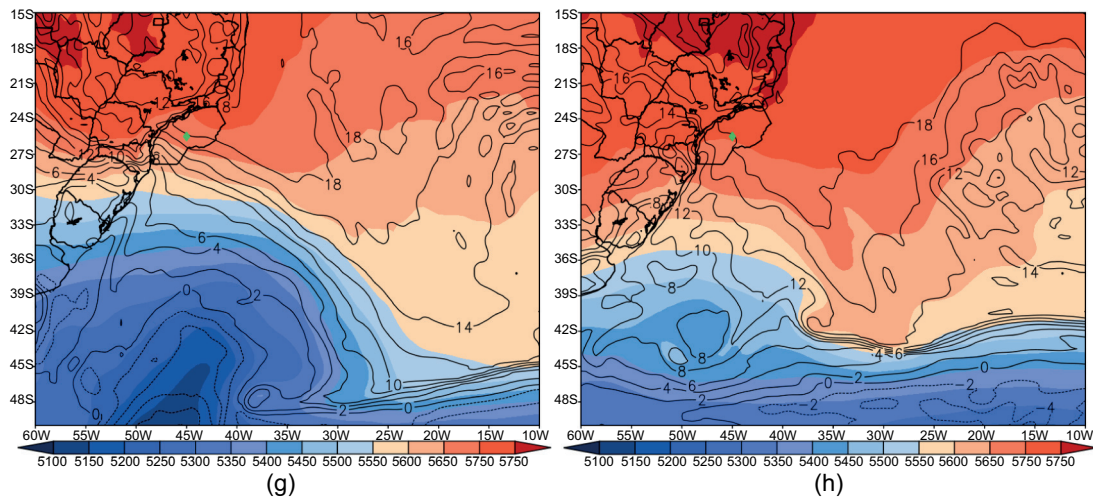


Fig. 7. (g) and (h) THC500_1000 (gpm, shaded) and DT2M ($^{\circ}\text{C}$, contour). Fields are for INTW Case (07/03/2018 at 18:00 UTC (left column) and MODW Case (05/12/2018 at 18:00 UTC (right column). Santos buoy location is indicated in the green diamond.

ocean and reaches the north of the Santos Basin in both cases. The cold air behind the cold front is colder and drier in the INTW Case (Fig. 7g). Nonetheless, the warm air forward the cold front is wetter and warmer in the MODW Case (Fig. 7h). The air masses differences in the INTW composite (Fig. 1c), which generates a strong gradient of THC500_1000, DT2M, and MSLP, are also noted in the INTW Case (Fig. 7g).

On a large scale, the INTW Case (Fig. 8a) shows negative anomalies in almost the whole mid-latitudes circle, even as in the INTW composite (Fig. 4a), indicating the negative SAM performance. Meanwhile, in the MODW Case (Fig. 8b), the anomalies are less intense and do not show the SAM well-configured performance. On the east coast of South America, a negative anomaly and a large trough extend from the south of South America to the South of Brazil in the INTW Case (Fig. 8a), similar to those observed in the INTW composite (Fig. 4a). They may have favored the system intensification and, consequently, the pressure gradient observed. In the MODW case (Fig. 8b), this anomaly is less intense and further away from the continent. Besides, the trough has a smaller amplitude than in the INTW Case as in the composite (Fig. 4b). There is a pattern with a lower wavenumber in the INTW Case than in the MODW Case (Fig. 8a, b) at higher latitudes, similar to that seen in the composites (Fig. 4). At high levels, it is

possible to observe the south quadrant winds over the east coast of South America and the Santos Basin in the INTW Case (Fig. 8c). In addition, the wavenumber in the INTW Case is smaller than in the MODW Case (Fig. 8c, d), as seen in the composites (Fig. 5). Figure 8c shows south quadrant winds over the coast, but they are more restricted to the southern region of Brazil. In Figure 8d, it is possible to observe a transition between winds from the south to the north quadrant in the north of the Santos Basin.

4. Conclusion

The present work aimed to identify the main atmospheric characteristics of the cold fronts that caused intense winds in the Santos Basin. Cases with W10M above the 99th percentile were considered INTW cases and those between the 70th and 90th percentiles as MODW cases. Most selected cases occurred in winter in INTW (seven out of 10 cases) and autumn in MODW (five out of 10 cases).

The composite analysis indicates that, for INTW cases, the post-frontal anticyclone that advances over the continent and the frontal trough that reaches the BS are more intense than in MODW, which caused a strong pressure gradient over the Santos Basin (up to $1.6 \times 10^{-3} \text{ Pa m}^{-1}$), with the isobars presenting an almost meridional position near the basin, generating

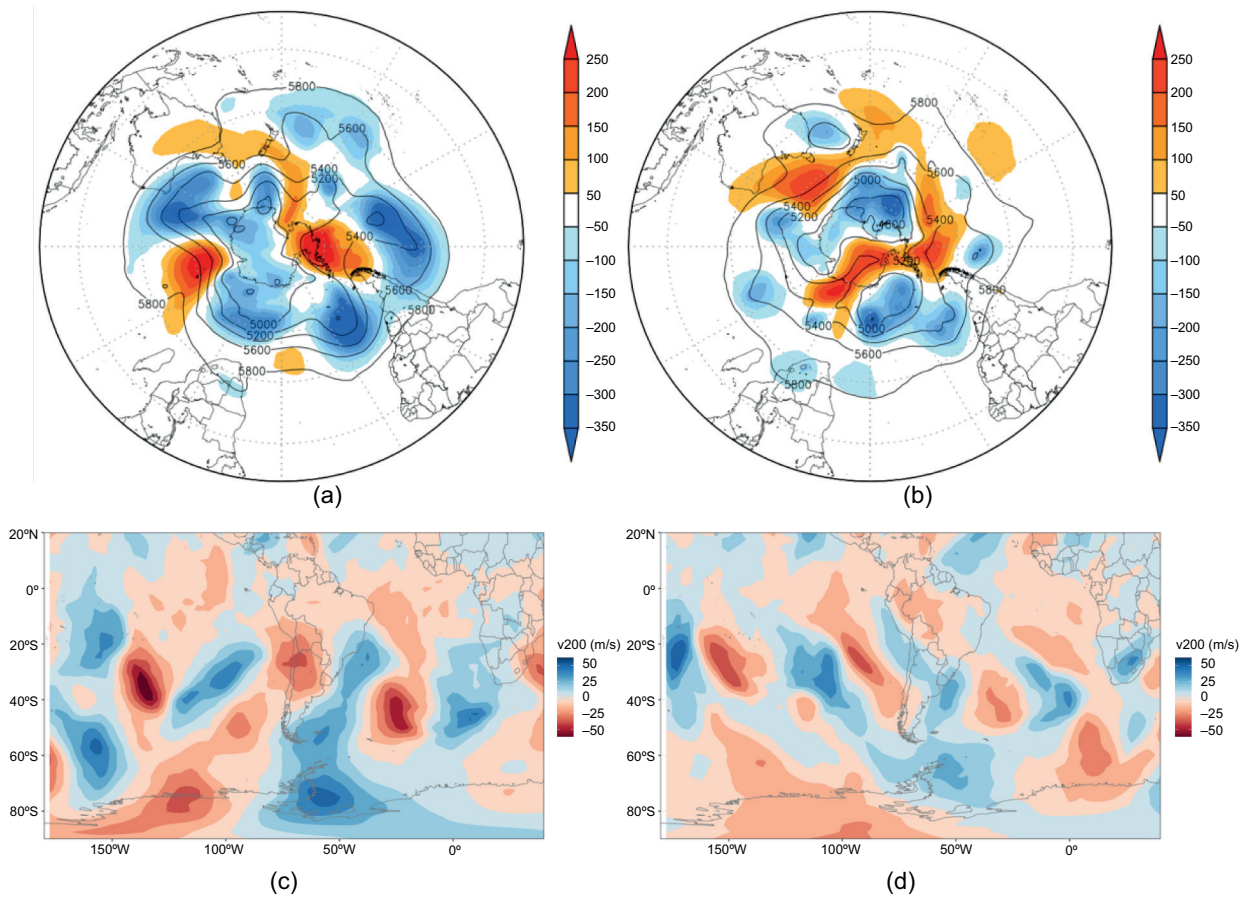


Fig. 8. Geopotential height (gpm, solid lines) and geopotential anomaly (gpm, shaded) at 500 hPa (top row) and v200 (bottom row) for: (a) and (c) INTW case (07/03/2018 at 18:00 UTC), (b) and (d) MODW Case (05/12/2018 at 18:00 UTC).

the strong winds recorded in the buoy. In addition, the baroclinic trough at medium and high levels has a greater amplitude than MODW and is over the study region. The air mass associated with the post-frontal anticyclone is colder and drier in INTW and goes further into the continent. Meanwhile, the air mass that acts on the inner part of the country and north of the Santos Basin is warmer and wetter, intensifying the THC500_1000 and DT2M gradient. It was also observed that the cold fronts were more continental in INTW since the strong THC500_1000 and DT2M gradient were over the continent.

On a large scale, there is a wave train from the Pacific to the Atlantic at medium and high levels, but anomalous centers shifted eastward in MODW relative to the INTW. Rossby wave trajectory analyses

using the raytracing method suggest that most waves leave from mid-latitudes in the South Pacific towards South America. In addition, this method indicates that some trajectories start closer to the continent with $K=2, 3$ in MODW. This corroborates what is observed in the composites, where the wavenumber is smaller in INTW ($K=2$), which may have favored the systems to be more continental in INTW.

Regarding the case studies, the analyses indicate that the main characteristics found in the respective composites are observed in the selected cases. For the INTW Case, a post-frontal anticyclone advance is higher than in the MODW Case. However, the frontal trough over the basin is less intense. As in the INTW composite, there is a baroclinic trough with great amplitude in medium and high levels, the advance

of a colder and drier air mass over Southern Brazil, and THC500_1000 and DT2M stronger gradients over the continent and ocean in the INTW Case. On a large scale, the wavenumber is smaller than in the MODW case, as in the composite.

It can be concluded that the cold fronts responsible for the generation of intense winds over the Santos Basin are associated with a great trough in medium and high levels and an intense post-frontal anticyclone, which contribute to a strong pressure gradient over the region. Wave trains from the Pacific with low wavenumbers ($K = 2$) favor the configurations found in the Atlantic for the SF that cause intense winds in the Santos Basin.

Acknowledgments

The authors thank Petrobras for supporting this research by means of the Research and Development Project, under the grant number 2018/00067-1.

References

- Andrade KM, Pinheiro HR, Dolif Neto G. 2015. Extreme precipitation episode in Rio de Janeiro: Synoptic analysis, numerical simulation and comparison among previous events. *Ciência e Natura* 37: 17-180. <https://doi.org/10.5902/2179460X16236>
- Andrade KM, Cavalcanti FA. 2018. Atmospheric characteristics that induce extreme precipitation in frontal systems over Southeastern Brazil during summer: Observations and atmospheric model simulation. *International Journal of Climatology* 38: 1-18. <https://doi.org/10.1002/joc.5744>
- Bonnet SM, Dereczynski CP, Nunes A. 2018. Caracterização Sinótica e Climatológica de Eventos de Chuva Pós-Frontal no Rio de Janeiro. *Revista Brasileira de Meteorologia*, 33: 547-557. <https://doi.org/10.1590/0102-7786333013>
- Brasil M. 2021. Escala Beaufort. Available at: https://www.marinha.mil.br/chm/sites/www.marinha.mil.br/chm/files/u2035/escala_beaufort.pdf (accessed on July 6, 2021).
- Caldas CF, Vasconcellos FC, Cavalcanti IFA, Carvalho NO, Lopes IDR. 2020. Impacto do gelo marinho antártico, do ENOS e do modo anular sul sobre as frentes frias na América do Sul. *Anuário do Instituto de Geociências* 43: 229-237. https://doi.org/10.11137/2020_4_229_237
- Cavalcanti IFA, Kousky V. 2009. Frentes frias sobre o Brasil. In: *Tempo e clima no Brasil*. Oficina de Textos, São Paulo, 135-147.
- Coelho CAS, de Oliveira CP, Ambrizzi T, Reboita MS, Carpenedo CB, Campos JLPS, Tomaziello ACN, Pampuch LA, Custódio MS, Dutra LMM, Da Rocha RP, Rehbein A. 2016. The 2014 southeast Brazil austral summer drought: Regional scale mechanisms and teleconnections. *Climate Dynamics* 46: 3737-3752. <https://doi.org/10.1007/s00382-015-2800-1>
- Dereczynski CP, Menezes WF. 2015. Meteorologia da Bacia de Campos. In: *Meteorologia e oceanografia*. Elsevier, 1-54. <https://doi.org/10.1016/B978-85-352-6208-7.50008-8>
- Dereczynski CP, Calado RN, Barros AB. 2017. Extreme rainfall in the city of Rio de Janeiro: History from the 19th Century. *Anuário do Instituto de Geociências* 40: 17-30. https://doi.org/10.11137/2017_2_17_30
- Dereczynski CP, Lopes ÍR, Carvalho NO, Silva MGJ, Grossman KS, Martins RP. 2019. Climatology of Espírito Santo and the northern Campos Basin, offshore southeast Brazil. *Anuário do Instituto de Geociências* 42: 386-401. https://doi.org/10.11137/2019_1_386_401
- Dolif G, Nobre C. 2012. Improving extreme precipitation forecasts in Rio de Janeiro, Brazil: Are synoptic patterns efficient for distinguishing ordinary from heavy rainfall episodes? *Atmospheric Science Letters* 13: 216-222. <https://doi.org/10.1002/asl.385>
- Escobar GCJ, Reboita, MS, Souza A. 2019. Climatology of surface baroclinic zones in the coast of Brazil. *Atmosfera* 32: 129-141. <https://doi.org/10.20937/ATM.2019.32.02.04>
- Franco RM-C, Menezes WF, Vasconcellos FC. 2020. Análise sinótica e de mesoescala de ventos intensos com impacto destrutivo em linhas de transmissão de energia elétrica no Paraná. *Revista Brasileira de Geografia Física* 13: 3177-3194. <https://doi.org/10.26848/rbgf.v13.07.p3177-3194>
- Hoskins BJ, Ambrizzi T. 1993. Rossby wave propagation on a realistic longitudinally varying flow. *Journal of Atmospheric Sciences* 50: 1661-1671. [https://doi.org/10.1175/1520-0469\(1993\)050%3C1661:RW-POAR%3E2.0.CO;2](https://doi.org/10.1175/1520-0469(1993)050%3C1661:RW-POAR%3E2.0.CO;2)
- Jones PW. 1999. First- and second-order conservative remapping schemes for grids in spherical coordinates. *Monthly Weather Review* 127: 2204-2210. [https://doi.org/10.1175/1520-0493\(1999\)127%3C2204:FASOC-R%3E2.0.CO;2](https://doi.org/10.1175/1520-0493(1999)127%3C2204:FASOC-R%3E2.0.CO;2)

- Lima KC, Satyamurty P, Fernández JPR. 2010. Large-scale atmospheric conditions associated with heavy rainfall episodes in Southeast Brazil. *Theoretical and Applied Climatology* 101: 121-135. <https://doi.org/10.1007/s00704-009-0207-9>
- Moura CRW, Escobar GCJ, Andrade KM. 2013. Padrões de circulação em superfície e altitude associados a eventos de chuva intensa na Região Metropolitana do Rio de Janeiro. *Revista Brasileira de Meteorologia* 28: 267-280. <https://doi.org/10.1590/S0102-77862013000300004>
- Petrobras. 2022. Bacia de Santos. Available at: <https://petrobras.com.br/pt/nossas-atividades/principais-operacoes/bacias/bacia-de-santos.htm> (accessed on August 17, 2021).
- R Core Team. 2021. R: A language and environment for statistical computing. R Foundation for Statistical Computing, Vienna, Austria. Available at: <https://www.R-project.org/> (accessed on June 21, 2021).
- Reboita MS, Ambrizzi T, Porfirio R. 2009. Relationship between the SAM and the SH atmospheric systems. *Revista Brasileira de Meteorologia* 24: 48-55. <https://doi.org/10.1590/S0102-77862009000100005>
- Reboita MS, da Rocha RP, Ambrizzi T, Sugahara S. 2010. South Atlantic Ocean cyclogenesis climatology simulated by regional climate model (RegCM3). *Climate Dynamics* 35: 1331-1347. <https://doi.org/10.1007/s00382-009-0668-7>
- Rehbein A, Ambrizzi T, Ibarra-Espinosa S, Dutra L. 2020. Raytracing: An R package for identification and tracking the atmospheric Rossby waves. R package version 0.1.0. Available at: <https://github.com/salvatirehbein/raytracing> (accessed on June 21, 2021).
- Saha S, Moorthi S, Wu X, Wang J, Nadiga S, Tripp P, Behringer D, Hou Y-T, Chuang H, Iredell M, Ek M, Meng J, Yang R, Mendez MP, van den Dool H, Zhang Q, Wang W, Chen M, Becker E. 2014. The NCEP Climate forecast system version 2. *Journal of Climate* 27: 2185-2208. <https://doi.org/10.1175/JCLI-D-12-00823.1>
- Satyamurty P, Nobre CA, Silva Dias PL. 1998. South America. In: *Meteorology of the Southern Hemisphere* (Karoly DJ, Vincent DG, Eds.). Meteorological Monographs. American Meteorological Society, Boston, 119-139. https://doi.org/10.1007/978-1-935704-10-2_5
- Vasconcellos FC, Cavalcanti IFA. 2010. Extreme precipitation over Southeastern Brazil in the austral summer and relations with the Southern Hemisphere annular mode. *Atmospheric Science Letters* 11: 21-26. <https://doi.org/10.1002/asl.247>
- Vasconcellos FC, Souza JN de. 2022. The anomalous wet 2020 southeast Brazil austral summer: Characterization and possible mechanisms. *Atmósfera* 35: 27-38. <https://doi.org/10.20937/ATM.52919>
- Wilks DS. 2006. *Statistical methods in the atmospheric sciences*. International Geophysics Series. Academic Press, San Diego.
- Yang GY, Hoskins BJ. 1996. Propagation of Rossby waves of nonzero frequency. *Journal of Atmospheric Sciences* 53: 2365-2378. [https://doi.org/10.1175/1520-0469\(1996\)053%3C2365:PORWON%3E2.0.CO;2](https://doi.org/10.1175/1520-0469(1996)053%3C2365:PORWON%3E2.0.CO;2)

Supplementary material

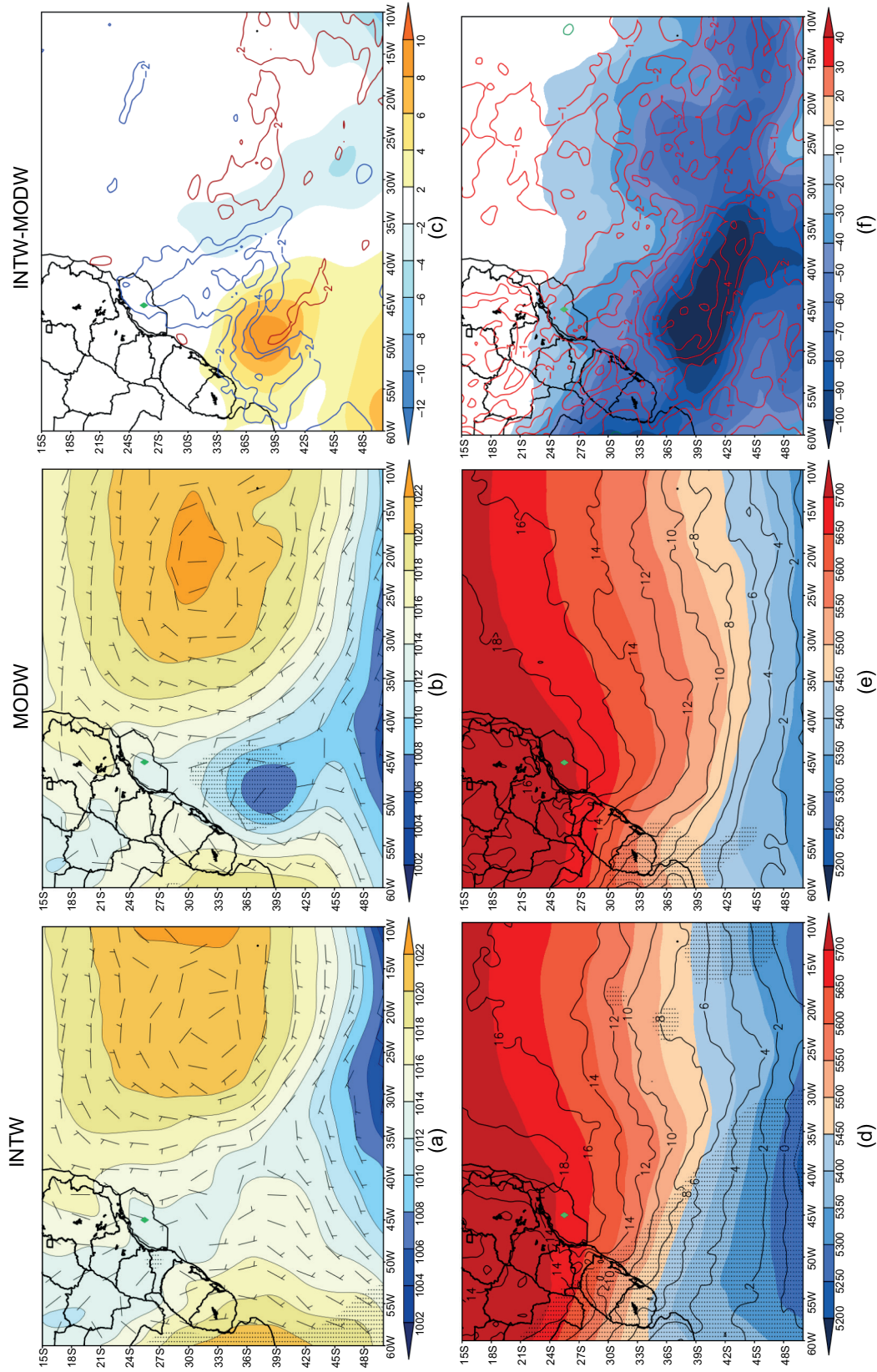


Fig. S1. MSLP (hPa, shaded) and W10M (m s^{-1} , barb) composites (top row); and THC500_1000 (gpm, shaded) and DT2M ($^{\circ}\text{C}$, contour) composites (bottom row), 24 h before the synoptic time closest to the occurrence of the most intense winds ($t = -24$) in each event. (a) and (d) INTW, (b) and (e) MODW, (c) and (f) INTW-MODW. c) W10M (m s^{-1} , contour) difference between INTW-MODW. Areas with 95% statistical significance in dots (t-Student test) for MSLP (top row) and layer thickness (bottom row). Santos buoy location is indicated in the green diamond.

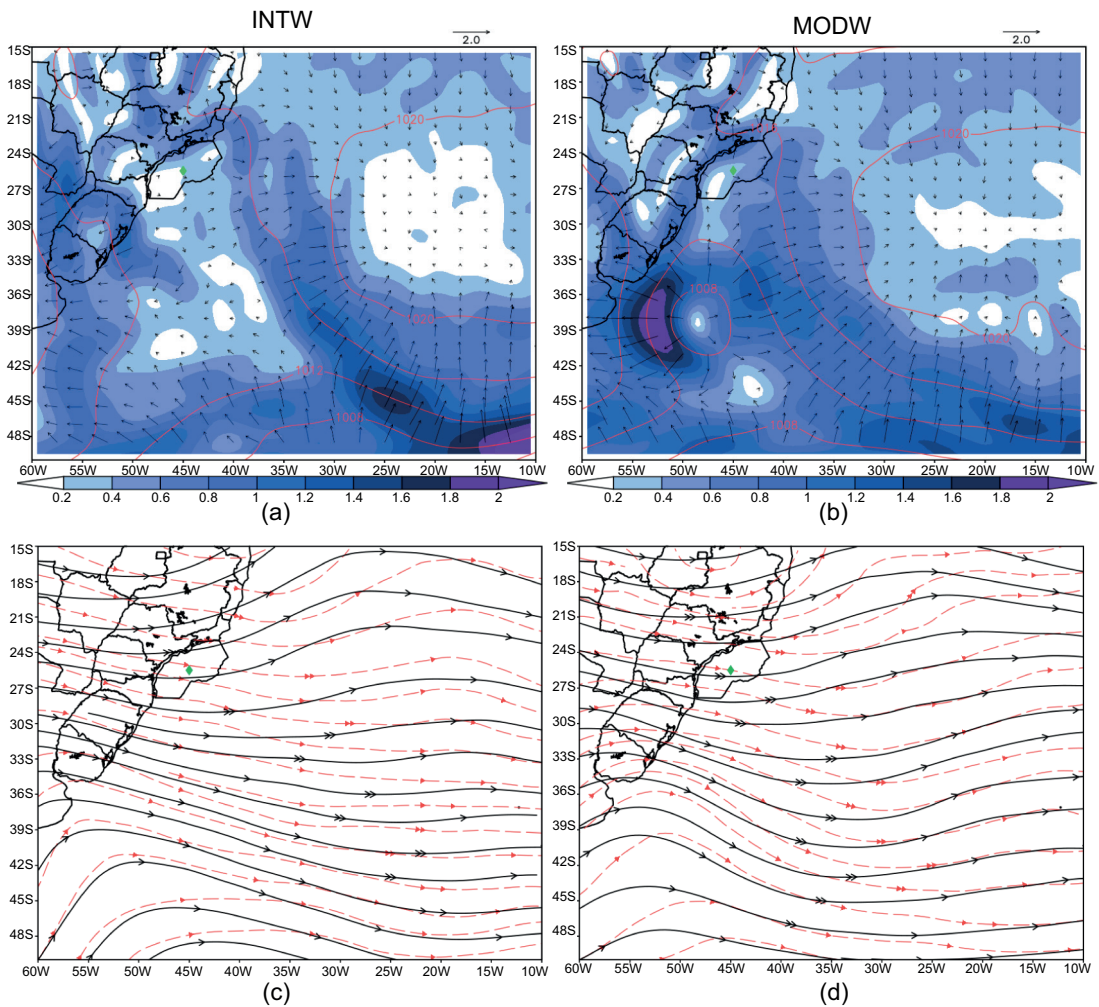


Fig. S2. Pressure gradient ($10^{-3} \text{ Pa m}^{-1}$, vector and shading) with MSLP (red line in hPa) composites (top row) and streamline at 500 hPa (dashed red) and 200 hPa (solid black) composites (bottom row), 24 h before the synoptic time closest to the occurrence of the most intense winds ($t = -24$) in each event. (a) and (c) INTW, (b) and (d) MODW. Santos buoy location is indicated in the green diamond.